J Mater Sci (2008) 43:2761–2770
DOI 10.1007/s10853-008-2486-4

(Cu, Fe, Co, or Ni)-doped tin dioxide films deposited by spray pyrolysis: doping influence on film morphology

G. Korotcenkov · V. Brinzari · I. Boris

Received: 8 October 2007 / Accepted: 18 January 2008 / Published online: 27 February 2008

Abstract The results of structural characterization of SnO_2 films doped by impurities such as Fe, Cu, Ni, and Co during spray pyrolysis deposition from 0.2 M $SnCl_4$–water solutions are presented. The change of parameters such as film morphology, the grain size, texture, and the intensity of X-ray diffraction peaks were controlled. For structural analysis of tested films, we used X-ray Diffraction, Scanning Electron Microscopy, and Atomic Force Microscopy techniques. It was shown that the doping promoted the change of the film morphology and the decrease of the SnO_2 grain size; however, these changes were not great. The doping influence becomes apparent more obviously for thin films and the films deposited at low temperatures ($T_{pyr} \sim 350$ °C). At higher pyrolysis temperatures ($T_{pyr} \sim 450$ °C), the influence of the doping on both the grain size and the film morphology was weakened. We concluded that used additives had dominant influence on the structural properties of SnO_2 at the initial stages of the film growth, as well as at the stages of twinning and agglomeration of the SnO_2 crystallites. It was shown that the increase in the contents of the fine dispersion phase in as-deposited film is an important consequence of the SnO_2 doping.

G. Korotcenkov (✉) · V. Brinzari · I. Boris
Technical University of Moldova, Chisinau,
Republic of Moldova
e-mail: ghkoro@yahoo.com

G. Korotcenkov
Korea Institute of Energy Research, Daejeon, Republic of Korea

Introduction

Recent researches have shown that simple (binary) metal oxides in many cases did not have a combination of properties, necessary for the fabrication of the gas sensors, satisfying the requirements such as high sensitivity and good selectivity at high temporal stability of operating characteristics [1–6]. It was established that those problems could be resolved by an optimization of the metal oxide matrix composition through doping by various additives [7–14]. The same approach was also widely used during a design of the metal oxide varistors with high nonlinearity of the current–voltage (I–V) characteristics [15, 16].

A conception of such approach is based on a statement that the appearance of elements with differing physical–chemical properties in the metal oxide matrix provides additional factors for influencing on the important parameters of the metal oxides [12, 13, 17, 18]. For example, the additives can change parameters of the metal oxides such as a concentration of charge carriers, chemical and physical properties of the metal oxide matrix, electronic and physical–chemical properties of the surface (energetic spectra of the surface states, energy of adsorption and desorption of surface species, the sticking coefficients, etc.), a catalytic activity, the surface potential, the height of inter-crystallite barriers, the phase composition, the size of crystallites, and so on [5, 19–27]. The appearance in the metal oxide matrix of a second phase even in a small quantity can change the conditions of basic oxide growth. It was found that certain additives, used during the metal oxide single crystal growth, can considerably change their crystal shape [28–31]. As a result of a special additive embedding, the magnetic properties of the metal oxides can be appreciably changed as well. It makes them very attractive for the spintronics and magnetic memory devices design [32–34].

However, it is necessary to note that the research in the field of material sciences of the doped metal oxides, especially in the form of thin films, is limited. This process is hampered by both the fragmentation of present information and sufficient difference in the conditions of synthesis and deposition used in various laboratories for preparation of doped metal oxides. Moreover, the main part of the results available in the literature is devoted to the study of the doping influence on the properties of the metal oxide powders and crystals, synthesized by various methods. As a result, there is no enough data for making any conclusion regarding the doping influence on both the structural parameters and the morphology of the metal oxide films. As it is known, the processes of metal oxide growth during chemical synthesis and film deposition from vapor phase have too many differences, and therefore we can not use knowledge obtained during ceramics study for prediction of the changes in thin film parameters during the doping process.

In this connection, the study of additives influence on the morphology of the SnO_2 films deposited by spray pyrolysis method was the main goal of the research presented in this article. The SnO_2 is one of the most used metal oxides for the design of gas sensors, smart windows, transparent electrodes, and room-temperature magnetic materials; therefore, the obtaining the above-mentioned information is very important for real applications of this material. Structural properties of the undoped SnO_2 films studied in this article were described earlier in detail in [35–37].

Experimental details

The SnO_2 films were deposited by spray pyrolysis from 0.2 M $SnCl_4$–water solutions. As it was shown in [35–38], the selected method has great advantages for deposition of SnO_2 films with controlled parameters. Studied films were deposited onto oxidized Si substrate at T_{pyr} = 350–370 °C or 450–475 °C. Those T_{pyr} were selected as deposition parameters, providing the attainment of an optimal SnO_2 film structure for the solid-state gas sensor design [5, 35, 36]. The rate of the solution flow during spray pyrolysis deposition was ~0.1 mL/s, which provided the rate of the SnO_2 films growth ~0.4 nm/s at T_{pyr} = 450 °C. The film thickness estimated by using laser ellipsometry varied from 40 to 400 nm. Films with thickness within the above-mentioned ranges are the most widely used for application in solid-state gas sensors.

Currently, many elements from III, V, VI, VII groups as well as 3-d transition metals were tested as additives for the SnO_2 properties' modification. However, in our experiment Fe, Cu, Co, and Ni were selected as doping additives. Their selection was conditioned by the fact that those impurities, on one hand, could influence the film structure [5, 28, 30, 31], and on the other hand, they may be used for synthesizing nanocomposites perspective for the design of the gas sensors, the varistors, and the diluted magnetic semiconductors [5, 14, 15, 16, 24, 25, 32–34, 39, 40]. The additives were embedded into a solution prepared for the spraying in the form of chlorides. The concentration of the doping elements in the sprayed solution varied from 0 to 16 at.%. As it was shown in above-mentioned references, the concentration of additives, optimal for the above-mentioned applications, is in the indicated concentration range.

X-ray Diffraction (XRD), Scanning Electron Microscopy (SEM), and Atomic Force Microscopy (AFM) were used for the structural characterization of the deposited films. XRD measurements were carried out by a Rigaku Rotaflex X-ray diffractometer with a rotating anode source, working with the Kα of the Cu. For the structural characterization, we used the $\theta/2\theta$ mode of measurements. The average size of the crystallites in the deposited films was estimated by Scherer's formula. For SEM measurements, we used the scanning electronic microscopes Philips XL30, and Stereoscan JS360 Cambridge Instruments with structural resolution ~0.3–0.4 nm. AFM images were obtained using MultiMode Scanning Probe Microscope with Nanoscope IIIa Controller of Digital Instruments. These measurements were carried out in contact scanning mode, using AS-0.5 scanner (scan rate 2 Hz; resolution 0.4 nm).

Results and discussions

General characterization

It is known that the limited solubility of many oxides in SnO_2 does not exceed 0.5–1.0 wt.% [41–43]. For example, according to [43], the solubility of CoO in SnO_2 is 0.5 mol.%, and further addition of CoO results in precipitation of Co_2SnO_4. Therefore, it seems that while using the doping at the level of 1–16 at.%, one should observe at the XRD patterns the appearance of additional peaks connected with X-ray diffraction at the crystal lattice of the second oxide phase. However, at the XRD patterns of the studied films, within the limits of the experiment error, we did not observe additional peaks, corresponding to other oxides even at concentrations of the doping additives, exceeding 16 at.% (see Figs. 1 and 2).

Regarding XRD patterns, directly related to SnO_2, one can say that the doping in the used concentration range does not change the general regularities of both the T_{pyr} and the film thickness influence on the shape of XRD patterns established in [35, 39]. It was found that as well as for the undoped SnO_2 films, having cassiterite structure, at XRD patterns of the doped SnO_2 films deposited at low T_{pyr} (350 °C), the peaks, conditioned by X-ray diffraction at the

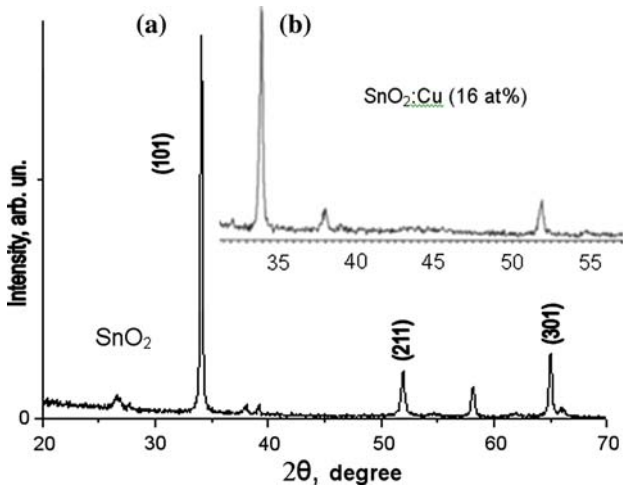

Fig. 1 Typical XRD patterns of (**a**) undoped and (**b**) doped SnO_2 films deposited at T_{pyr} = 350 °C ($d \sim 250$ nm)

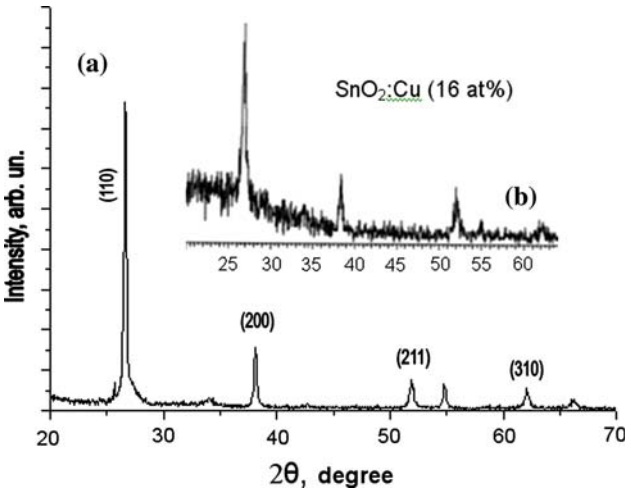

Fig. 2 Typical XRD patterns of (**a**) undoped and (**b**) doped SnO_2 films deposited at T_{pyr}= 450 °C ($d \sim$ 50–70 nm)

(101) plane, dominate (see Fig. 1), while at $T_{pyr} = 450$ °C, the peaks connected with X-ray diffraction at (110), and (200) planes just start dominating at XRD patterns (see Fig. 2). The doping only changes a little bit the ratio of those peaks intensities. The absence of strong additives influence on the XRD patterns of the SnO_2 films deposited by the spray pyrolysis was also observed in [44] for SnO_2 doped by Ni, and in [45] for SnO_2 doped by Cu (4 at.%).

Meanwhile, the data of the electron probe microanalysis (EDAX) testify that embedded additives are really present in the oxide matrix in the quantity, close to the one, introduced to the initial solution prepared for spraying. For example, while the concentration of the doping elements in the sprayed solution equaled 16 at.%, the concentration of Co, Cu, and Fe in the SnO_2 films, estimated by using EDAX method, was 10–15, 10–12, and 10–13 at.%, respectively. Tested films were deposited at T_{pyr} = 450 °C.

Thus, EDAX results testify that the second oxide must be present in the SnO_2 matrix. However, the absence of characteristic XRD peaks, caused by the presence of the second metal oxide phase, allows to conclude that those oxides are in a very fine dispersed state. As it was established by various researches, only for the crystallites with size exceeding 1–3 nm, well-defined peaks should become apparent in the XRD patterns. This conclusion is in accordance with the results of the research given in [22, 40, 46]. The study of a two-phase systems, in which the concentration of the second oxide phase was small in comparison to the basic oxide, has shown that the second phase, as a rule, was the fine dispersed one, being formed on the surface of the basic oxide's grains. It means that the grains of second oxide phase are smaller than the grains of basic oxide and really can have size as small as 1–3 nm. As it will be shown in section "The doping influence on the SnO_2 grain size," the grain size of basic SnO_2 oxide in deposited films varied in the range 10–50 nm.

The doping influence on the SnO_2 grain size

As it was shown in [5, 14–16], the usage of the additives during the process of sol–gel synthesis of the SnO_2 powders with the following annealing at T_{an} = 700–950 °C inhibits the grain size increase in comparison with the undoped material. Usually the doped SnO_2 powders after annealing had the grain size 2–5 times smaller than the undoped ones. During our research it was established that the doping of tin dioxide during the spray pyrolysis deposition promotes also either the change of the film morphology or the grain size decrease. The results of the doping influence on the morphology of SnO_2 films deposited at T_{pyr} = 450 °C are presented in Figs. 3 and 4.

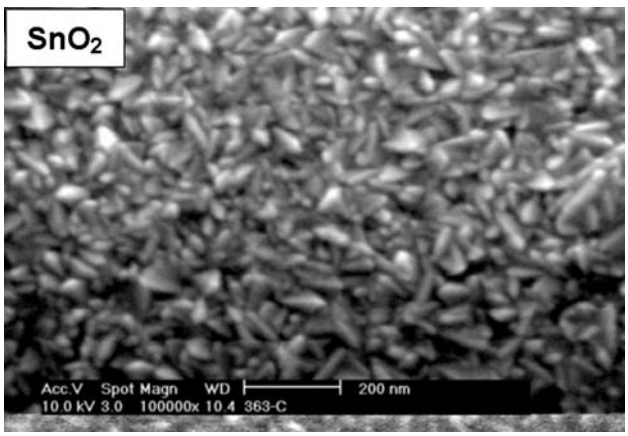

Fig. 3 SEM image of undoped SnO_2 film ($d \sim 120$ nm) deposited by spray pyrolysis on oxidized Si substrate at T_{pyr} = 450 °C

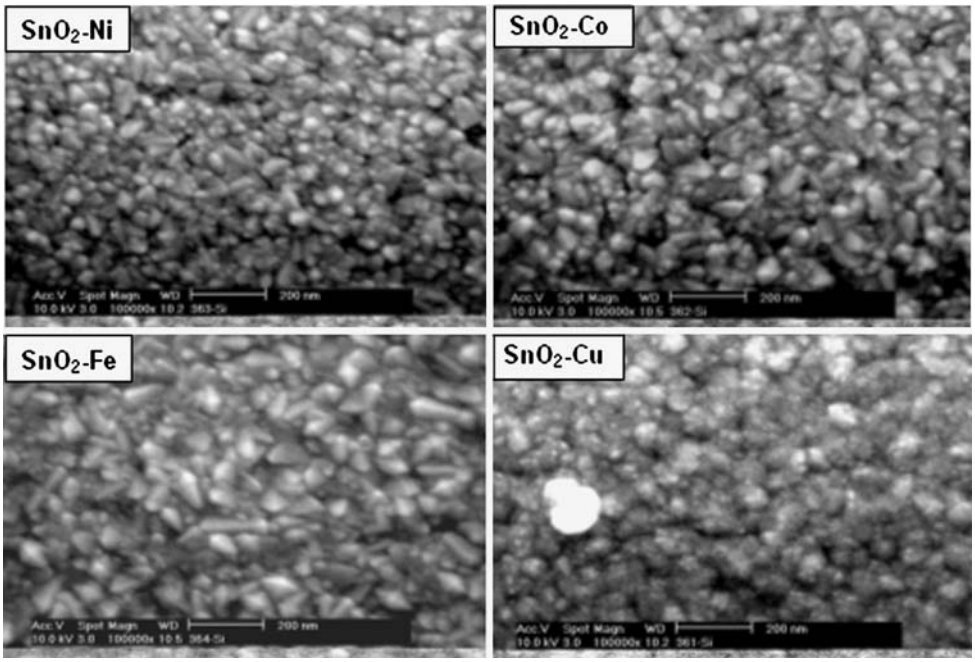

Fig. 4 Influence of doping by (**a**) Ni, (**b**) Co, (**c**) Fe, and (**d**) Cu (16 at.%) on SEM images of SnO_2 films ($d \sim 120$ nm) deposited by spray pyrolysis on oxidized Si substrate at $T_{pyr} = 450$ °C

Table 1 Doping influence on the average size of grains and agglomerates in SnO_2 films ($d \sim 120$ nm), deposited at $T_{pyr} \sim 450$ °C

Doping element	Grain size (nm)				Agglomerate size (nm)	
	AFM	SEM	XRD		AFM	SEM
			(110)	⟨t⟩		
Undoped	23 ± 6	23 ± 7	32	27	60–90	30–90
Cu	18 ± 6	18 ± 7	25	18	70–120	100–150
Co	24 ± 6	23 ± 6	26	25	70–120	60–80
Ni	22 ± 5	21 ± 5	27	22	60–90	50–80
Fe	22 ± 8	22 ± 6	21	23	60–80	40–90

The concentration of additives in sprayed solution equaled ~16 at.%

⟨t⟩, average grain size; (110), average size of grains in (110) plane parallel to substrate

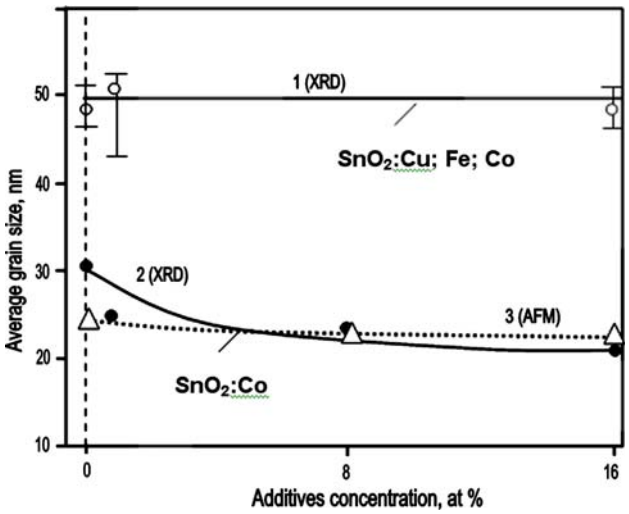

Fig. 5 Influence of additives concentration on SnO_2 the grain size in films with thickness equaled (1) ~400 nm, and (2, 3) ~120 nm: $T_{pyr} = 450$ °C: (1, 2)— the grain size estimated by XRD method; (3)—by AFM method

However, the decrease of the grain size, estimated on the basis of XRD data and SEM images, was not so considerable as it was expected, based on the results obtained for the SnO_2 powders [14–16]. In spite of a strong influence on the film morphology, the XRD data testified that the average grain size was only slightly changed. Mentioned peculiarity was established for the results, obtained by using both XRD and SEM methods. Looking at the data, presented in Table 1 and Fig. 5, one can see that the change in the average grain size did not exceed 40% from the initial crystallite size, even for SnO_2 with maximum doping influence on film morphology. This change was greatly dependent on both the T_{pyr} and the film thickness. A considerable decrease of the grain size was observed only for the thin enough films (see Fig. 5). This effect will be considered in more detail in section "Dependence of the doping influence on the film parameters."

Moreover, we found that for the attainment of a noticeable result in the change of film morphology it was necessary to embed the additives at the level of >10 at.%. However, the study of gas-sensing characteristics of the SnO_2 sensors fabricated on the basis of the doped material has shown that those concentrations of additives (>10 at.%) appreciably exceeded the level of concentrations at which the

Table 2 The decrease of conductivity response of SnO_2 sensors on the basis of doped films with high concentration of additives in comparison with sensors fabricated on the basis of undoped materials

Additive	K_1 (~1 ppm O_3)	K_2 (1000 ppm H_2)
Fe (16 at.%)	30–100	3–5
Co (16 at.%)	$>10^3$	3–10
Cu (16 at.%)	3×10^2–10^3	15–20
Ni (16 at.%)	$\sim 10^2$	5–10

SnO_2 films were deposited at $T_{pyr} \sim 450$ °C and had thickness that equaled ~40–60 nm

K_1—the ratio of conductivity responses (S) to ozone of undoped and doped SnO_2-based sensors; K_2—the same ratio for sensor response to hydrogen. K = S(undoped)/S(doped)

Table 3 Doping influence on intensity of X-ray diffraction at (110) plane

T_{pyr} (°C)	d (nm)	Doping element	XRD intensity (110)
350	250 ± 20	–	80 ± 5
		Cu	52 ± 5
450	120 ± 10	–	356 ± 20
		Cu	158 ± 15
		Fe	189 ± 15
		Co	308 ± 20
		Ni	365 ± 20
450	400 ± 20	–	1660 ± 50
		Cu	1620 ± 50
		Fe	1670 ± 50
		Co	1400 ± 40

Doping additives had concentration that equaled 16 at.%

improvement of the sensor response to both reducing and oxidizing gases was observed [5, 8, 14, 19]. For doping additives used the maximum of sensor response to H_2 and ozone was observed only when the concentration of additives equaled 1–5 at.%. The excess of this concentration threshold leads to the sharp decrease in the sensor response. The results, confirming this statement, are presented in Table 2. These results were obtained for sensors on the basis of doped SnO_2 fabricated using thin film technology [47, 48]. It is seen that the conductivity response of the heavily doped SnO_2 films, for example to ozone, decreased in 10–10^3 times in comparison with the undoped films. It means that the attempt to improve gas-sensing characteristics through the decrease of grain size induced by special doping is not always the best solution for the achievement of optimal gas sensor parameters. In this case, the change of the grain boundary properties caused by segregation of second oxide phase on the surface of basic oxide grains, in all probability, may have more powerful influence on the sensor response than the grain size decrease. Such an approach for explanation of the gas-sensing characteristics of the SnO_2- and In_2O_3-doped films we used in [5, 26, 39].

One should note that the weak influence of the doping additives in the concentration range of 0–16 at.% on the SnO_2 grain size is in agreement with the statement well known in metallurgy [29, 31, 49]. According to the conclusions made in [29, 31, 49], the inhibition of the grain growth in the presence of the second phase takes place when the average domain size is comparable with the average interparticle distance. As it was concluded earlier, in our case, the grain size of the second phase is considerably smaller than this distance. Besides, it is necessary to take into account that the mechanisms of the grain growth during the film deposition and the high-temperature treatments of already synthesized SnO_2 powders are different. During the thermal treatment of synthesized powders, the grains of the second oxide located between the SnO_2 grains can really prohibit from the Sn transfer from the one crystallite to the another one; during the film deposition, a small grains of the second oxide cannot appreciably limit the delivery of the components of the SnO_2 pyrolysis reaction to the surface of already existing SnO_2 crystallites.

According to the data of XRD measurements (see Table 1) obtained for (110) SnO_2 plane, the doping by iron provides maximum decrease of the grain size. At the same time, according to the data of SEM and AFM measurements, the doping by copper shows the maximum influence on the films morphology (see Figs. 3 and 4). Moreover, we established that the doping by Cu is accompanied by the maximum decrease in the intensity of the X-ray diffraction peaks (see Table 3). As it follows from the results presented in Table 3, the doping by Cu is accompanied by a decrease in the intensity of X-ray diffraction peaks up to 2 times. The doping by Fe provides about the same decrease in the intensity of the X-ray diffraction peaks. During doping by cobalt and especially by nickel, the decrease in the intensity of the X-ray diffraction peaks is considerably smaller.

The analysis of obtained results, showing a noticeable decrease in the intensity of the X-ray diffraction peaks against a background of the negligible change of average crystallites size, estimated by using XRD method, allowed to make the following conclusion: observed effect is a consequence of the increase in as-deposited-doped SnO_2 films contents of the fine dispersed phase of just SnO_2, which similarly to fine dispersed phase of the second oxide phase does not give contribution at XRD patterns. We assume that the second oxide creates additional nucleation centers for the SnO_2 growth, and therefore, the growth of SnO_2 film during deposition takes place not only due to the increasing in the size of crystallites incipient at primary stage of growth, but also due to the appearance of new

grains, having considerably smaller size in comparison with already present crystallites that appeared at the initial stages of the SnO_2 films' growth. We assume that this SnO_2 amorphous-like phase fills up the inter-crystallite space and promotes the densification of metal oxide matrix, i.e., the decrease of gas penetrability of deposited doped SnO_2 films. Schematic diagram of doped SnO_2 films' structure, inclusive of fine-dispersed phases, is shown in Fig. 6.

So, we believe that additives such as copper and iron promote the maximal increase of the contents of such SnO_2 fine dispersion phase. AFM images of as-deposited SnO_2:Cu films presented in Fig. 7 confirm our conclusion. One can see that the SnO_2 grains in AFM images of the SnO_2:Cu films, having according to our point of view the maximum contents of the fine dispersion phase, possess the diffuse image edges. Under our model, the diffuse image of grains' edges appears due to low resolution of SEM technique, which does not allow discriminating the fine dispersed grains located on the surface of basic oxide's crystallites. At the same time, the grains in AFM images of the SnO_2:Ni films, characterized according to our data by a minimal contents of this fine dispersed phase, have a clear delineated image edges.

It is necessary to note that a possibility of the simultaneous presence in tin dioxide films of both crystallites and the fine dispersion amorphous-like phase was experimentally proved in [50]. The authors of this paper have observed near 50% of such amorphous-like phase in the SnO_2 films deposited by CVD method. In our prior works we also denoted the chance of the presence of such amorphous-like phase in the undoped SnO_2 films deposited at low pyrolysis temperatures.

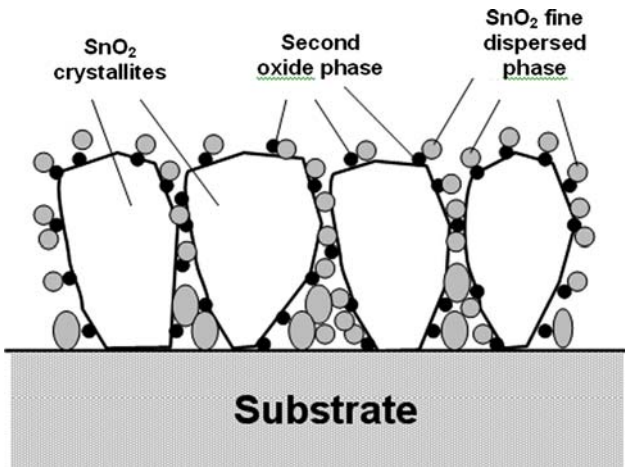

Fig. 6 Schematic diagram of the structure of SnO_2-doped films

After analyzing the obtained results we concluded that at certain conditions, including the conservation of both the measurement conditions and film thickness invariable (without changes), the intensity of X-ray diffraction peaks can be considered as a parameter, characterizing the crystallinity of the studied material. The smaller the intensity of X-ray diffraction peaks poorer is the crystallinity of studied metal oxide , i.e., the content of the fine dispersion amorphous-like phase in the studied film is greater.

One should note that the presence of great amount of the fine dispersion phase, which does not participate in shaping of XRD patterns, makes us to be careful with any quantitative evaluations made on the basis of XRD data. In this case we obtain information mainly about the grains, giving the contribution in XRD patterns, i.e., first of all about the crystallites incipient at the initial growth stage and grown through the whole film thickness. Insufficiently high resolution of SEM technique can also be a reason for the errors in the determination of a real crystallite size. At poor resolution, especially in the case when the fine dispersed phase filling out the intercrystallite space, is presented in the oxide, the agglomerates could be recognized as separate grains. Such an error in the SEM images interpretation one can meet often in many publications, including our early work [51], where the dense agglomerates in the In_2O_3 films deposited at low pyrolysis temperatures were recognized as separate crystallites.

Dependence of the doping influence on the film parameters

Comparing the results obtained while studying various SnO_2 films, one can conclude that the additives influence

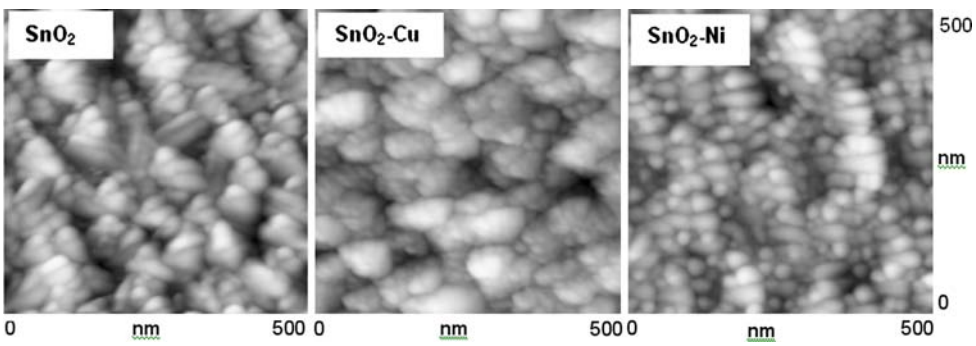

Fig. 7 AFM images (500 × 500 nm) of (**a**) undoped and doped by (**b**) Cu, and (**c**) Ni (16 at.%) SnO_2 films ($d \sim 120$ nm) deposited at $T_{pyr} = 450$ °C

on both the film morphology and the grain size is more pronounced for the films deposited at the low temperature.

As we indicated earlier for the films deposited at $T_{pyr} \sim 450$ °C, the influence of the additives on the film structure is not so substantial as for films deposited at $T_{pyr} \sim 350$ °C is concerned.

Our experiments have also shown that the additive influence on the film structure depends on the film thickness. For example, the additives' influence was stronger for the thin films. If for the films with thickness ~400 nm both the average grain size and the X-ray diffraction peak intensity practically did not change during the doping; for films with thickness <100 nm this influence was clearly shown (see Fig. 5 and Table 2). It means that the influence of the doping additives is more substantial at the initial stages of the film growth, when the rate of the growth in many respect is determined by the presence of nucleation centers. As we mentioned earlier, the presence of second oxide can promote the generation of a larger number of nucleation centers for SnO_2 growth. Thus from our experiments one can conclude that the additive influence is different at various stages of the film growth. The comparison of AFM images of SnO_2, deposited on alumina glass ceramics and oxidized Si single crystal, confirmed our conclusion. We found that in case of the SnO_2 film with the thickness ~40–50 nm, the grain size in films deposited on the surface of alumina glass ceramics was noticeably smaller than for the films deposited on the oxidized Si substrate. When the thickness was more than 100 nm, the difference in morphology of the SnO_2 films deposited on the different substrates was minimal. It means that the doping during spray pyrolysis deposition indeed can be an effective tool for structural engineering of the thin metal oxide films.

The doping influence on the SnO_2 film agglomeration

Analyzing data of XRD and SEM measurements, we established a difference in the grain sizes estimated for the SnO_2 thick films on the basis of XRD and SEM methods. The grain size estimated by using SEM images for the thick SnO_2 films was noticeably bigger that the one calculated on the basis of XRD data. For example, if estimations on the base of SEM images of the undoped and Fe-doped SnO_2 films with the thickness ~400 nm ($T_{pyr} = 450$ °C) (see Fig. 8) result in the grain sizes in the range from 40 to 130 nm, the analysis of XRD data gives an average grain size that equals ~40 nm.

In [35] we supposed that such big difference among the results of conducted estimations could be conditioned by peculiarities of the grain growth and by the presence of a mechanical strains inhomogeneously distributed over the film thickness. However, after more careful comparative analysis of SEM and AFM images we concluded that observed distinction in addition to the above-mentioned factors is conditioned by the SnO_2 crystallites' inclination to the twinning. We have found experimental confirmation of this conclusion in [52] devoted to detailed study of the SnO_2 film structure by High Resolution Transmission Electrum Microscopy (HRTEM) method. It was found that many crystallites of SnO_2 are multiply twinned withtwinning planes, parallel to one of the (101) lattice planes.

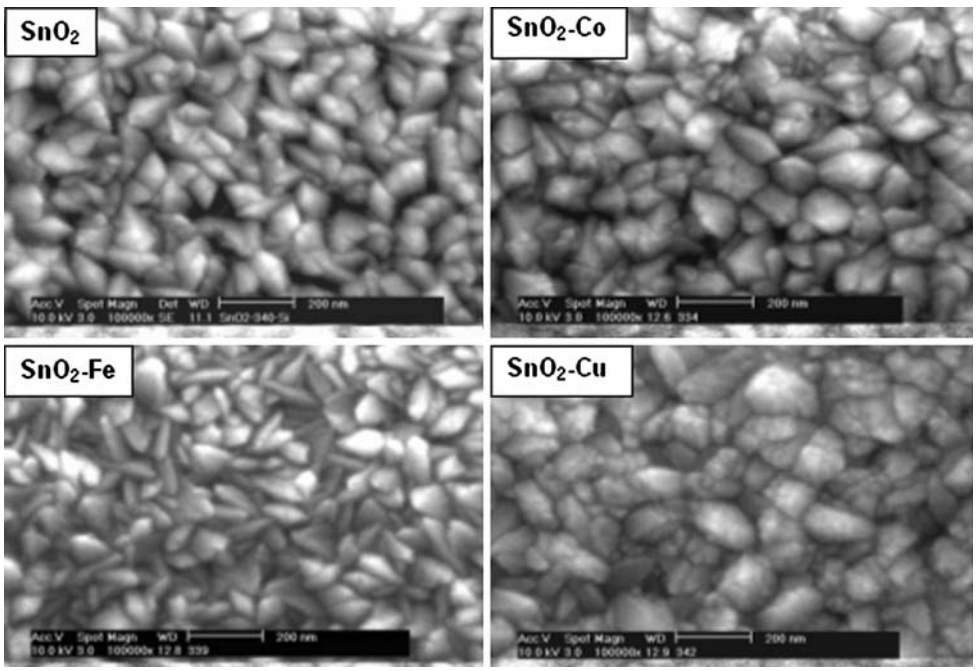

Fig. 8 SEM images of (**a**) undoped and doped by (**b**) Co, (**c**) Fe, and (**d**) Cu (16 at.%) SnO_2 films ($d \sim 400$ nm) deposited by spray pyrolysis on oxidized Si substrate at $T_{pyr} = 450$ °C

If, at SEM images, the twined crystallites looked like a monolithic formation, for X-ray diffraction such a formation seemed to be as two or more individual crystallites with smaller size. In other words, the large formations observed at SEM images are some kind of the agglomerates. They can be selected by the uncharacteristic shape and by the presence of faceting, which are not peculiar to the individual crystallites. Agglomerates become apparent more clearly at SEM images of SnO_2 doped by copper and cobalt (see Fig. 8). For SnO_2 doped by nickel and iron, it is not so clearly shown. However, the use of AFM method, having better resolution, has shown that even for those films, deposited at $T_{pyr} < 450$ °C, the formations observed at SEM images were agglomerates (see Fig. 9). At that it relates to the films with the thickness of 100 nm (Figs. 3 and 4) as well as to the films with thickness of 400 nm (see Fig. 9). The examination of AFM images testifies that agglomerates, depending on the size and the nature of the doping impurity, include two or more crystallites.

It was established that the agglomerates shape depends on T_{pyr}. At $T_{pyr} \sim 350$ °C agglomerates have the shape of spherulites and their form does not depend on the doping (see Fig. 10). At $T_{pyr} \sim 450$ °C the agglomerates acquire diamond shape with clearly shown cutting, characteristic for the individual crystallites (see Fig. 8). In other words, at those T_{pyr} we observe some kind of self-assembling. From our point of view, it is a very interesting result requiring further study.

The analysis of SEM images presented in the Fig. 8 also shows that the agglomerates shape depends on the nature of the doping impurity used. If the iron influenced weakly on the agglomerates shape, especially for the thick films, the additives of nickel, cobalt, and especially copper changed the agglomerates shape considerably. In the case of doping by cobalt, the agglomerates become wider in comparison with agglomerates in the undoped SnO_2. At the doping by copper they are being transformed from a diamond shaped into formations with the shapes, which cannot be described as some geometrical ones.

The agglomerates size depends on the doping additives as well. Agglomerates in the Cu-doped SnO_2 films are the biggest ones. If in the undoped SnO_2 films with the thickness ~ 120 nm ($T_{pyr} = 450$ °C), the agglomerate size was ranged within the limits of 60–90 nm; for the copper-doped SnO_2 films the agglomerate size would reach 100–150 nm. For the films doped by other dopants, the agglomerate size varied from 40 to 90 nm.

So, strong influence of the doping impurity on the film morphology allows us to conclude that in spite of a weak doping influence on the crystallite size, especially for the

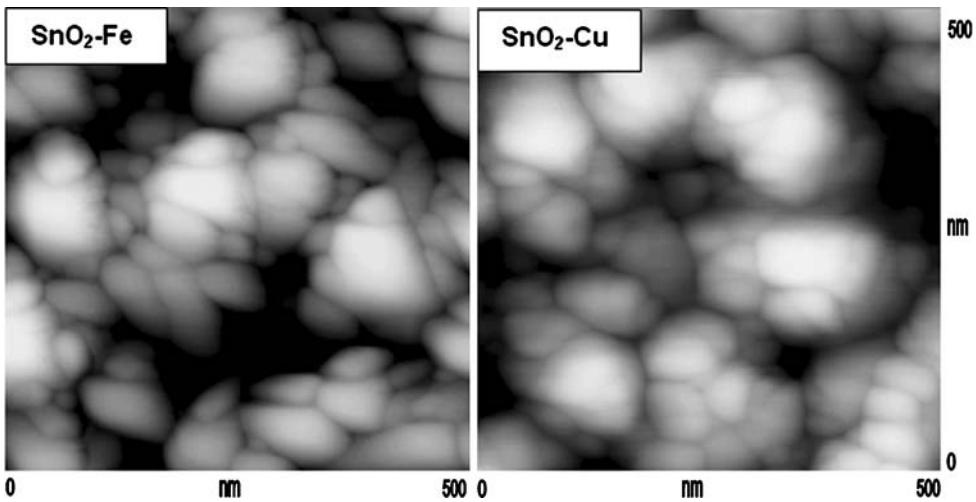

Fig. 9 AFM images (500 × 500 nm) of SnO_2 films deposited at $T_{pyr} = 450$ °C ($d \sim 400$ nm) doped by (**a**) Fe and (**b**) Cu (16 at.%)

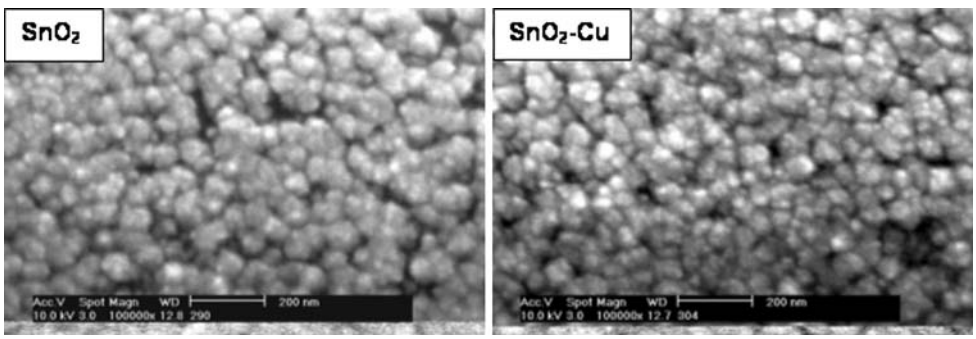

Fig. 10 SEM images of (**a**) undoped and (**b**) Cu-doped (16 at.%) SnO_2 films deposited at $T_{pyr} = 350$ °C. Films had thickness that equaled ~ 80 nm

thick films (see Fig. 4), the role of the doping additives in the film morphology forming is a substantial one. In all probability besides the initial stage of growth, the nature of the doped additives also determines the specificity of both twinning and the crystallite agglomeration in the growing SnO_2 film.

It is necessary to note that the formation of dense agglomerates could be a good explanation of the reasons for the gas-sensing characteristics' change observed in SnO_2-based sensors at the increase of the film thickness. We suppose that in the films formed from dense agglomerates, not the intercrystallite contacts, but the interagglomerate ones may control both the resistance and the sensor response. In such films the area of the intercrystallite contacts in dense agglomerates may be too large in comparison with the area of the interagglomerate contacts. Besides that, in the presence of dense agglomerates, the intercrystallite diffusion can also become a process, controlling the kinetics of sensor response [5]. In other words, the intercrystallite diffusion of oxygen and target gas inside dense agglomerates indeed can be the main reason for the increase of either the response and recovery times observed during the gas detection by metal oxide sensors. The importance of agglomeration process for correct understanding gas-sensing effects was shown earlier by us [53].

Conclusion

Conducted research has shown that tin dioxide doping by Fe, Co, Ni, and Cu (0–16 at.%) during the spray pyrolysis deposition promotes both the change of the film morphology and the decrease of grain size. However, the decrease of the grain size, estimated on the basis of XRD data and SEM images, was not great. The influence of doping becomes apparent more obviously for the films with small thickness and for films deposited at low temperatures ($T_{pyr} \sim 350$ °C). At higher pyrolysis temperatures ($T_{pyr} \sim 450$ °C) the doping influence on both the grain size and the film morphology is being weakened. Based on the analysis of observed effects, we concluded that during spray pyrolysis deposition the additives exert main influence on the film structure at the initial stages of the film growth, as well as at the stage of twinning and agglomeration of the SnO_2 crystallites. It was shown that the increase in the contents of the fine dispersion phase in the deposited film, becoming more apparent for the SnO_2 films doped by copper and iron, is an important consequence of the SnO_2 doping. It was assumed that big crystallites of doped SnO_2 are covered by a layer of such fine dispersed phase.

Acknowledgements This work was supported by Supreme Council of Science and Advanced Technology of the Republic of Moldova in the frame of special State Program. Authors are thankful also to Prof. J. Schwank for helping in XRD and SEM characterization of studied samples. G. Korotcenkov is thankful to Korean Brain Pool Program for the support to his research as well.

References

1. Gopel W, Hese J, Zemel JN (eds) (1991) Sensors: a comprehensive survey. Chemical and biochemical sensors, part 1, vol 2. VCH, Germany
2. Gopel W, Scherbaum KD (1995) Sens Actuators B 26–27:1
3. Morrison SR (1986) In: Aucouturier JL (ed) Proceedings of the 2nd international meeting on chemical sensors, Bourdeaux, France, 7–10 July, p 39
4. Moseley PT, Tofield BC (eds) (1987) Solid state gas sensors. Adam Hilgen, Bristol
5. Korotcenkov G (2005) Sens Actuators B 107:209
6. Korotcenkov G (2007) Mater Sci Eng B 139:1
7. Choi SD, Lee DD (2001) Sens Actuators B 77:335
8. Ivanovskaya M, Bogdanov P, Faglia G, Nelli P, Sberveglieri G, Taroni A (2001) Sens Actuators B 77:268
9. Ferroni M, Carotta MC, Guidi V, Martinelli G, Ronconi F, Sacerdoti M, Traversa E (2001) Sens Actuators B 77:163
10. Madou MJ, Morrison SR (1989) Chemical sensing with solid state devices. Academic Press, Inc., San Diego
11. McAleer JF, Moseley PT, Norris JOW, Williams DE, Tofield BC (1988) J Chem Soc Faraday Trans 1 84:441
12. Meixner H, Lampe U (1996) Sens Actuators B 37:198
13. Yamazoe N, Miura N (1992) In: Yamauchi N (ed) Chemical sensors technology, vol 4. Kodansha, Tokyo, pp 20–41
14. Yamazoe N, Kurokawa Y, Seiyama T (1983) Sens Actuators 4:283
15. Wang JF, Chen HC, Su WB, Zang GZ, Wang B, Gao RW (2006) J Alloy Compd 413:35
16. Qi P, Wang JF, Su WB, Chen HC, Zang GZ, Wang CM, Ming BQ (2005) Mater Chem Phys 92:578
17. Gleiter H (1992) Nanostruct Mater 1:1
18. Gleiter H (2000) Acta Mater 48:1
19. Kanazawa E, Sakai G, Shimanoe K, Kanmura Y, Teraoka Y, Miura N, Yamazoe N (2001) Sens Actuators B 77:72
20. Shimizu Y, Matsunaga N, Hyodo T, Egashira M (2001) Sens Actuators B 77:35
21. Skala T, Veltruska K, Moroseac M, Matolinova I, Korotcenkov G, Matolin V (2003) Appl Surf Sci 205:196
22. Szezuko D, Werner J, Oswald S, Behr G, Wetzing K (2001) Appl Surf Sci 179:301
23. Wang W, Xu C, Wang X, Liu Y, Zhan Y, Zheng C, Song F, Wang G (2002) J Mater Chem 12:1922
24. Yamaura H, Jinkawa T, Tamaki J, Moriya K, Miura N, Yamazoe N (1996) Sens Actuators B 35–36:325
25. Yamaura H, Moriya K, Miura N, Yamazoe N (2000) Sens Actuators B 65:39
26. Korotcenkov G, Boris I, Brinzari V, Luchkovsky Y, Karkotsky G, Golovanov V, Cornet A, Rossinyol E, Rodriguez J, Cirera A (2004) Sens Actuators B 103:13
27. Carreno NLV, Maciel AP, Leite ER, Lisboa-Filho PN, Longo E, Valentino A, Probst LED, Paiva-Santos CO, Schreiner WH (2002) Sens Actuators B 86:185
28. Kawamura F, Takahashi T, Yasui I, Sunagawa I (2001) J Cryst Growth 233:259
29. Palatnik LS, Fuks MI, Kosevich VM (1972) Mechanism of formation and substructure of condensed films. Nauka, Moscow (in Russian)

30. Panchapakesan B, De Voe DL, Widmaier MR, Cavicchi R, Semancik S (2001) Nanotechnology 12:336
31. Kawamura F, Yasui I, Sunagawa I (2001) J Cryst Growth 233:517
32. Hong NH (2006) J Magn Magn Mater 303:328
33. Yan L, Pan JS, Ong CK (2006) Mater Sci Eng B 128:34
34. Rodriguez-Torres CE, Fabiana Cabrera A, Sanchez FH (2007) Phys B: Condens Mater 389:176
35. Korotcenkov G, Cornet A, Rossinyol E, Arbiol J, Brinzari V, Blinov Y (2005) Thin Solid Films 471:310
36. Korotcenkov G, Brinzari V, Dibattista M, Schwank J, Vasiliev A (2001) Sens Actuators B 77:244
37. Brinzari V, Korotcenkov G, Schwank J, Lantto V, Saukko S, Golovanov V (2002) Thin Solid Films 408:51
38. Korotcenkov G, Brinzari V, Schwank J, Cerneavschi A (2001) Mater Sci Eng C 19:73
39. Korotcenkov G, Dibattista M, Schwank J, Brinzari V (2000) Mater Sci Eng B 77:33
40. Pagnier T, Boulova M, Galerie A, Gaskov A, Lucazeau G (2001) Sens Actuators B 71:134
41. Dufour LC, Nowotny J (eds) (1988) Surface and near-surface chemistry of oxide materials. Elsevier, Amsterdam
42. Nowotny J (1988) Solid State Ionics 28–30:1235
43. Kim BC, Jung JI, Lee JH, Kim JJ (2001) Solid State Ionics 144:321
44. Liu CM, Fang LM, Zu XT, Zhou WL (2007) Chin Phys Soc (IOP) 16:95
45. Chimbeu CM, Van Landschoot RC, Schoonman J, Lumbreras M (2007) J Eur Ceram Soc 27:207
46. Varela JA, Cerri JA, Leite ER, Longo E, Shamsuzzoha M, Bradt RC (1999) Ceram Int 25:253
47. Korotcenkov G, Blinov I, Ivanov M, Stetter JR (2007) Sens Actuators B 120:679
48. Korotcenkov G, Brinzari V, Dmitriev S (1999) Sens Actuators B 54:202
49. Thompson CV (2000) Annu Rev Mater Sci 30:159
50. Jimenez VM, Espinos JP, Caballero A, Contreras L, Fernandez A, Justo A, Gonzalez-Elope AR (1999) Thin Solid Films 353:113
51. Korotcenkov G, Cerneavschi A, Brinzari V, Cornet A, Morante J, Cabot A, Arbiol J (2002) Sens Actuators B 84:37
52. Pan X, Zheng JG (1997) In: Im J, Yalisove S, Adams B, Zhu Y, Chen F-R (eds) Polycrystalline thin films-structure, texture, properties and applications III, MRS symposium proceedings, vol 472. Boston, USA, p 87
53. Korotcenkov G, Macsanov V, Tolstoy V, Brinzari V, Schwank J, Faglia G (2003) Sens Actuators B 96:602